FRMPD2: a novel GluN2A-interacting scaffold protein in synaptic excitatory transmission

Xi Lu[1], Haiqing Zhang[1], Yun Li[1], Ruijiao Zhou[1], Miaoqing He[1], Yuanlin Ma[1], Xin Tian[1], Xuefeng Wang[1, 2*].

Affiliations:

1: Department of Neurology, Chongqing Key Laboratory of Neurology, The First Affiliated Hospital of Chongqing Medical University, 1 Youyi Road, Chongqing 400016, China

2: Center of Epilepsy, Beijing Institute for Brain Disorders, 10 Xitoutiao, Youanmen, Fengtai District, Beijing 100069, China.

*: The corresponding author: Xuefeng Wang, Email: wxfcqmu@163.com

Address correspondence to Xuefeng Wang, Department of Neurology, The First Affiliated Hospital, Chongqing Medical University, 1 Youyi Road, Chongqing 400016, China.

Abstract

The scaffold proteins FRMPD2 is localized at the basolateral membranes of polarized epithelial cells and associated with tight junction formation. But the expression and function of FRMPD2 in vivo remain unknown. Here, we found that postsynaptic FRMPD2 effectively alters the neuronal excitability by regulating NMDARs-component excitatory synaptic transmission in adult hippocampus. FRMPD2 anchors the NMDAR subunit GluN2A at the synapses without changing the total NMDAR expression. By using of Co-IP, Pull Down and SPR, the second PDZ (PDZ2) domain of FRMPD2 direct and binds to the C-terminus of GluN2A. Moreover, Ferm domain of FRMPD2 directly interacts with actin filaments and modifies excitatory synapse morphogenesis, further strengthen neuronal excitatory transmission. In particular, FRMPD2 mediates the behavioral and field potential phenotypes of epilepsy, a brain disorder of excitatory/inhibitory imbalance. Our study discover that a novel scaffold protein FRMPD2 regulates synaptic excitatory in a PDZ2 domain- and Ferm domain-dependent manner in adult hippocampus.

Keywords: dendritic spines/ excitatory synapses/ NMDAR/ PDZ domain/ scaffold protein

Introduction

Scaffold proteins contain several modular protein interaction domains within their structure, and they bind to various interacting proteins, such as ion channels, neurotransmitter receptors, adhesion molecule, microtubule, filamentous actin (F-actin)(Anzai et al, 2002; Durand et al, 2012; Elias et al, 2007; Hruska-Hageman et al, 2002; Kim et al, 2004; Sala et al, 2001; Schultz et al, 1998). They strongly contribute to the organization of synaptic signalling complexes, and the clustering of surface receptors and ion channels, and they participate in the dynamic trafficking of vesicle transport and coordinate cytoskeletal dynamics(Feng et al, 2009). FRMPD2 (also named Gm626) is a novel scaffold protein that consists of an N-terminal KIND domain, a Ferm (band 4.1, ezrin, radixin, and moesin) domain and three C-terminal PDZ (PSD-95/Discs-large/ZO1) domains(Lipinski et al, 2012; Stenzel et al, 2009). FRMPD2 is reported to localize in the basolateral membranes of polarized epithelial cells and is associated with tight junction formation and immune response(Lipinski et al, 2012; Stenzel et al, 2009). However, there are few studies investigating FRMPD2 in vivo and the expression and function of FRMPD2 in nervous system remain unknown.

Inspired by multiple domains in its structure, FRMPD2 is predicted to play a critical role in neuronal excitation. PDZ domain-containing proteins are involved in neuronal excitatory by trafficking neurotransmitter receptors to plasma membrane(Kim & Sheng, 2004). Ferm domain-containing proteins are reported to recruit actin-regulatory proteins(Yang et al, 2009), and the F-actin cytoskeleton is

essential for neuronal morphogenesis and synaptic connectivity(Bourne et al, 2008; Lei et al, 2001). Thus, FRMPD2 may be implicated in the regulation of neuronal excitation or morphogenesis in a PDZ- or Ferm-dependent manner.

In this paper, we first reported that postsynaptic scaffold protein FRMPD2 activated neuronal excitability in adult hippocampus by mediating the N-methyl-d-aspartic acid (NMDA) receptors-component excitatory synaptic transmission. FRMPD2 anchored the GluN2A subunit of NMDA receptors (NMDARs) to the synapses by directly binding the second PDZ (PDZ2) domain to the C-terminus of GluN2A. FRMPD2 further regulated maturation of dendritic spines. At last, FRMPD2 mediated the susceptibility of epilepsy, a brain disorder of excitability(Kwan et al, 2011). Our study shed light on a novel scaffold protein FRMPD2 mediate synaptic excitatory and modulate epileptic seizures via directly anchoring synapses GluN2A subunits.

Results

1. Expression patterns of the FRMPD2 protein.

The FRMPD2 protein was expressed in a restricted manner in some organs including the brain, eyes, testes and lungs (Supplementary Fig 1A), and was enriched in a more widespread manner in various brain regions, including the cortex, hippocampus and cerebellum, in addition to the ependymal cells lining the ventricles (Supplementary Fig 1B, C).

When immunofluorescence staining was performed in mouse cortex and the hippocampus Cornu Ammonis 1 (CA1) region, FRMPD2 was localized in microtubule-associated protein 2 (MAP2)-positive neuronal dendrites and another major scaffold protein, PSD95 (postsynaptic marker) (Supplementary Fig 1D, E). Synaptosomes in the hippocampus were isolated by ultracentrifugation, and the FRMPD2 protein was detected in the postsynaptic density (PSD) fraction, but not in the presynaptic fraction or non-synaptic synaptosomal fraction (Supplementary Fig 1F).

2. Effects of FRMPD2 on NMDA receptor-mediated excitatory synaptic transmission

PDZ domain-containing proteins are involved in neuronal excitatory by interacting and trafficking neurotransmitter receptors(Kim & Sheng, 2004). We tested that whether postsynaptic FRMPD2 containing three PDZ domains affects neuronal excitatory. Whole cell patch-clamp electrophysiology was performed in CA1 pyramidal neurons in mouse hippocampal slices at 14 days after lentivirus vector (LV)

injection of mice that was used to knockdown or overexpress FRMPD2. LV-encoding green fluorescent protein (GFP) was detected in the mouse hippocampus (Supplementary Fig 2A). At 2 and 6 weeks post-LV injection, the FRMPD2 protein levels of the hippocampus in FRMPD2 knockdown mice (shFRMPD2) was almost 40 percent less than in scramble controls (shFRMPD2-Scr). FRMPD2 protein levels were significantly higher in shFRMPD2-Res mice that were injected with shRNA plus overexpression LV in the hippocampus than in FRMPD2 knockdown mice. The FRMPD2 protein in FRMPD2 overexpression mice (FRMPD2-OE) was 1.9-2.1 times higher than in negative controls (FRMPD2-OE NC) (Supplementary Fig 2B). These findings suggest that FRMPD2 protein levels in the hippocampus were effectively modulated by LV injection.

We firstly analyzed the effect of FRMPD2 on spontaneous action potential (AP) in CA1 pyramidal neurons. The frequency of spontaneous AP in FRMPD2 knockdown mice reduced by 71 percent compared with the scramble control. AP frequency of FRMPD2 overexpression mice was 2.28 times faster than in the negative control (Supplementary Fig 3A). To further explore the contribution of glutamate excitatory receptors and/or inhibitory synaptic inputs contribute to the increase in neuronal hyperactivity induced by FRMPD2, α-amino-3-hydroxy-5-methyl-4-isoxazole propionic acid (AMPA) receptor (AMPARs) component or NMDAR component mEPSCs, and miniature inhibitory postsynaptic currents (mIPSCs) of pyramidal neurons in the CA1 region of the hippocampus were recorded. The two types of ionotropic glutamate receptors, AMPARs and NMDARs,

present at postsynaptic membrane of excitatory synapses mediate almost all synaptic transmission in the brain(Bredt et al, 2003; Valtschanoff et al, 2001). There was no significant difference in AMPAR mEPSCs (Supplementary Fig 3B) or mIPSCs (Supplementary Fig 3C) after FRMPD2 knockdown or overexpression. However, the mEPSC amplitude, but not the frequency, of NMDAR mEPSCs was decreased in FRMPD2 knockdown mice compared with scramble controls, and increased in FRMPD2 overexpression mice compared with negative controls (Fig 1A).

To verify the changes of mEPSCs, NMDAR-mediated evoked EPSCs (eEPSCs) were measured. Firstly, the input-output curve of NMDAR eEPSCs (Fig 1B) verified that FRMPD2 enhanced the postsynaptic efficacy of NMDAR responses (Shen et al, 2010). As shown in Fig 1C, the amplitudes of NMDAR currents were significantly lower in the FRMPD2 knockdown than in the scramble controls. There was no significant difference in evoked AMPAR currents between the FRMPD2 knockdown and overexpression groups, in line with data of AMPAR component mEPSCs. In particular, to determine whether GluN2A and/or GluN2B component currents contributed to the observed changes in NMDAR eEPSCs, selective antagonist for GluN2A (NVP-AAM077) and GluN2B (Ro25-6981) were used (Fig 1D). The amplitude of GluN2A-sensitive currents of the FRMPD2 knockdowns was decreased by 65 percent compared with the scramble groups, and amplitude of GluN2A currents of overexpressing FRMPD2 mice was 2.38 times higher than of the negative controls. Interesting, the GluN2B component-mediated currents were not changed after FRMPD2 knockdown or overexpression. These results suggested that FRMPD2

strengthens GluN2A -mediated NMDARs synaptic transmission.

Because presynaptic release at postsynaptic glutamate receptors also contribute to synaptic excitatory transmission, we analyzed the paired-pulse ratio (PPR), a reliable index of the contribution of presynaptic vesicles release to excitatory postsynaptic currents(Zucker et al, 2002). There was no significant difference in PPR values between the FRMPD2 knockdown and overexpression results and those in the corresponding control groups (Fig 1E), indicating that presynaptic vesicles release is not responsible for the FRMPD2-mediated changes in mEPSCs

3. Effects of FRMPD2 anchoring GluN2A at synapses.

To correlate electrophysiological changes with biochemical alterations in synaptic NMDAR, we performed immunoblotting using hippocampal synaptosomal and total lysates. As shown in Fig 2A, the synaptic GluN1 and GluN2A were significantly fewer in the FRMPD2 knockdown mice than in the scramble mice, and higher in the FRMPD2 overexpression mice than in the negative controls. The synaptic GluN2B and total protein levels of GluN2A, GluN2B and GluN1 were not affected by FRMPD2. Immunofluorescence staining was also used to test for co-localization between FRMPD2 and GluN2A at postsynaptic membranes, which were marked by PSD-95 in hippocampal CA1 areas (Fig 2B).

The extreme C-terminus of the NMDAR subunits provides a mechanism for trafficking NMDAR subunits in postsynaptic membrane by interacting with PDZ proteins (Bard et al, 2010; Kim & Sheng, 2004). We performed co-immunoprecipitation (Co-IP) and GST pull-down assays to detect whether the

three PDZ domains of FRMPD2 interact with NMDAR subunits. In vivo, co-immunoprecipitation of FRMPD2 with GluN1 and GluN2A, but not GluN2B were detected in the lysates of mice hippocampus (Fig 2C). A GST fusion protein bearing the PDZ2 domain but not the first PDZ or third PDZ domain pulled down endogenous GluN1 and GluN2A, but not GluN2B from mice hippocampus in vivo. The full-length GluN1, GluN2A and GluN2B proteins tagging with GFP were generated in translation experiments in vitro, GST-PDZ2 pulled down full-length GluN2A, but not GluN1 and GluN2B (Fig 2D). However, the GST-PDZ2 fusion protein did not pull down GluN2A proteins from the cells transfected with a form of GFP-GluN2A that lacked a set of ten C-terminal amino acids (Fig 2D).

The binding abilities of FRMPD2-isolated PDZ2 domain to the GluN2A and GluN2B C-terminus was measured using surface plasmon resonance (SPR) analyses. The binding capacity of the FRMPD2 PDZ2 domain to bind to the wild type GluN2A C-terminus (KKMPSIESDV) and wild type GluN2B C-terminus (EKLSSIESDV) yielded a K_D (dissociation constant) value of 0.31μM and 0.25mM, respectively (Fig 2E,F), whereas no binding was observed between the mutant GluN2A C terminus (KKMPSIEADK) (Fig 2G) and the FRMPD2 PDZ2. These results supported the direct interaction of C terminus of GluN2A to PDZ2 of FRMPD2.

To further explore potential sites for binding between GluN2A and FRMPD2, we first obtained the crystal X-ray structure of the PDZ2 domain(Supplementary Fig 4A) of the mouse homologue of FRMPD2 (PDB ID: 5ZDS) (Supplementary Table 1). The crystal structure was solved by PHENIX with the template PDZ2 domain

structure of tyrosine phosphatase PTP-BL (PDB ID: 1VJ6) (Supplementary Fig 4B) with 63% identity(Adams et al, 2010; Gianni et al, 2006). In the template structure (Supplementary Fig 4C), there was a peptide that is a C-terminal (HSGSYLVTSV) of tumor suppressor protein APC, binding to β2 strand and α2 helix. The residues V(0) and T(-2) of the peptide formed critical hydrophobic interactions with residues L25, I27, L85, V29, and V65 of the template PDZ2 structure(Gianni et al, 2006). These residues were highly conserved in the FRMPD2 PDZ2 crystal structure, as shown by the alignment (Supplementary Fig 4D).

The results shown so far reveal that FRMPD2 affects NMDAR-mediated excitatory postsynaptic currents by anchoring GluN2A subunits at postsynaptic membranes. This activity is achieved by an interaction of the FRMPD2 PDZ2 domain to the GluN2A C-terminus.

4. Effects of FRMPD2 on the formation of excitatory synapses in hippocampus CA1 area.

Ferm domain-containing proteins are reported to recruit actin-regulatory proteins(Yang et al, 2009), and the F-actin cytoskeleton is essential for neuronal morphogenesis and synaptic connectivity(Bourne & Harris, 2008; Lei et al, 2001). We further evaluated the effect of FRMPD2 on the synaptic ultrastructure of CA1 hippocampal neurons by electron micrograph (Fig 3A). First, we assessed the number of excitatory (asymmetric) synapses, inhibitory (symmetric) synapses and presynaptic vesicles(Weeks et al, 2007). There were no differences in the numbers of excitatory synapses (Fig 3B), inhibitory synapses (Fig 3C) and presynaptic vesicles (Fig 3D)

after FRMPD2 knockdown or overexpression, consistent with our earlier electrophysiology data, indicating that FRMPD2 does not affect the frequency of mEPSC, mIPSCs or PPR values(Beique et al, 2003; Beique et al, 2006).

The length and thickness of the postsynaptic density (PSD) are primarily correlated with the number of glutamate receptors anchoring at individual synapses and this also closely related to the magnitude of mEPSCs (Sheng et al, 2007). Hence, PSD (measured along the postsynaptic membrane) length and thickness were calculated in mice after FRMPD2 knockdown or overexpression. The PSD was shorter and thinner in the FRMPD2 knockdowns mice but longer and thicker in FRMPD2 overexpression mice than in the corresponding controls (Fig 3E, F). These results suggested that FRMPD2 is critically requirement for PSD size enlargement.

We next quantitatively assessed the contact length of synapses which is closely related to spine head morphology in 2D electron micrographs. Contact length was defined as the length of the postsynaptic membrane in register with the presynaptic terminal was determined from the set of synapses used to measure PSD lengths (Harris et al, 2012). The contact length was shorter in FRMPD2 knockdown mice but longer in FRMPD2 overexpression mice than in the corresponding controls (Fig 3G). These results indicate that FRMPD2 is probably associated with dendritic spine morphology modifications.

Dendritic spines of neurons are the location of 90% excitatory synapses and contain the postsynaptic machinery, including glutamate receptors, scaffold proteins and actin cytoskeleton(Bourne & Harris, 2008). Hence, we tested that whether

FRMPD2 regulates the spines density and morphogenesis. Golgi staining was performed to determine the density and morphology of both apical and basal dendritic spines in hippocampal CA1 pyramidal neurons obtained from FRMPD2 overexpression or knockdown mice (Fig 3H). Spines are notably classified as "thin", "stubby", "mushroom" and " filopodia" based on various morphological characteristics (as illustrated in Fig 3I). Mature spines ("mushroom") have an enlarged head and a larger, more complex PSD that contains a higher density of glutamate receptors, resulting in a higher sensitivity to glutamate than in immature spines ("thin", "stubby" and " filopodia")(Bourne & Harris, 2008). We measured the numbers of mature and immature spines. There was an obvious reduction in mature spines numbers and an increase in immature spines numbers in CA1 hippocampal neurons in FRMPD2 knockdown mice. Conversely, the density of mature spines in mice overexpressing FRMPD2 was higher than in the negative controls, while the number of immature spines was reduced (Fig 3J). These data supported the view that FRMPD2 plays a role in spines maturation and density modulations.

5. Binding of the FRMPD2 Ferm domain to F-actin.

Ferm domain proteins have been reported to interact with F-actin that is closely associated with the NMDAR trafficking and dendritic spines morphogenesis(Bourne & Harris, 2008; Lei et al, 2001; Yang et al, 2009). Then, we tried to find whether the Ferm domain of FRMPD2 binds to F-actin. We transfected Flag-FRMPD2 constructs with or without a Ferm domain into HEK293T (Fig 4A) and SYHY-5Y (Fig 4B) cells, and then stained the cells for F-actin using rhodamine phalloidin. The full length of

FRMPD2 constructs with a Ferm domain (WT) colocalized with F-actin. Deleting the FRMPD2 Ferm domain (ΔFerm) eliminated its colocalization with actin, but the Ferm domain (Ferm) alone was required for actin colocalization. A quantification analysis showed that F-actin colocalization was significantly lower in the FRMPD2 ΔFerm-transfected cells than in those transfected with either FRMPD2 WT or Ferm (Fig 4C). Finally, we used an F-actin co-sedimentation assay, and the results showed that the Ferm domain of FRMPD2 binds directly to F-actin (Fig 4D). These results suggested that the FRMPD2-mediated morphological changes in dendritic spines probably depend on an interaction between the FRMPD2 Ferm domain and F-actin.

6. Modulation of FRMPD2 in epilepsy susceptibility.

The NMDAR subunit GluN2A has been powerfully implicated in the development of epilepsy, a disease that manifests as strong recurrent excitatory connections in the hippocampus(Kwan et al, 2011; Lemke et al, 2013). Because FRMPD2 was proved to mediate GluN2A-containing excitatory synaptic transmission in the hippocampus, we further explored whether FRMPD2 is involved in the regulation of epilepsy susceptibility.

Chronic pentylenetetrazol (PTZ) and kainic acid (KA)-induced epilepsy models were used. FRMPD2 protein levels were significantly higher in epileptic patients (Fig 5A, B) as well as in both the hippocampus and neocortex of epileptic mice than in the corresponding controls (Fig 5C-F). To further explore whether FRMPD2 modulates epilepsy susceptibility, behavioral and local field potential (LFP) studies were performed in two chronic epileptic animal models. Behavioral observation performed

in PTZ induced models showed that daily seizure scores were lower in FRMPD2 knockdown mice than in scramble controls (Fig 5G). More specifically, the FRMPD2 knockdown mice exhibited a lower total number of seizures and longer induced latency than were observed in the scramble controls (Fig 5H, I). In a behavioral analysis of KA-induced mice, the frequency of spontaneous recurrent seizures (SRSs) was lower and SRS latency was longer in FRMPD2 knockdown mice than in scramble controls(Fig 5J, K). Seizure-like events (SLEs) were recorded on EEGs performed in KA-induced mice (Fig 5O, P), while the FRMPD2 knockdown mice presented less numerous SLEs and had a shorter duration of SLE and a longer SLE interval time than were observed in the scramble controls(Fig 5L-N).

These behavioral results suggested that FRMPD2 modulates susceptibility to epilepsy by changing the duration, frequency and number of seizures.

Discussion

In our report, we identified a novel scaffold protein FRMPD2, and explored its physiological contribution to the modulation of excitatory synaptic electrophysiological function as well as excitatory synaptic formation (Fig 6). Scaffold proteins traffic and target of glutamate receptors(Elias & Nicoll, 2007; Lau et al, 2007) or sodium channels(Hruska-Hageman et al, 2002; Schultz et al, 1998) to the plasma membrane, and are involved in neuronal excitatory. Scaffolding proteins are also well-characterized for the regulation of dendritic spine morphology through coordinating cytoskeleton dynamic(Durand et al, 2012; Lee et al, 2016). Mature dendritic spines with numerous postsynaptic glutamate receptors are tightly correlated with strength of excitatory synapses(Chen et al, 2011). In general, there is little scaffolding proteins not only directly bind to receptors to govern excitatory synaptic function, but also directly bind to F-actin to control excitatory synaptic formation. For example, Shank proteins can bind to several actin-regulatory proteins, but they indirectly associate with type I metabotropic glutamate receptors via Homer protein(Durand et al, 2012). However, FRMPD2 interdependently enhance neuronal excitatory by the two isolate pathways.

While NMDAR-mediated and AMPAR-mediated transmission are both affected by PDZ proteins, but the FRMPD2 was not essential for AMPA-component excitatory transmission in adult hippocampus. It is seems that the binding of glutamate receptors by PDZ proteins appears to change with development in a glutamate receptor-specific manner(Beique et al, 2006; Elias et al, 2008). Knockout

of PSD-95 reduces AMPAR synaptic transmission with little effects on NMDARs in mature neurons(Beique et al, 2006). Interesting, mice deficient MAGUKs family members PSD-93, PSD-95 and SAP-102 had modestly reduced NMDAR EPSCs at CA1 neurons(Elias et al, 2006), suggesting the potential existence of other PDZ proteins that act independently of the MAGUKs family that regulate the targeting of PDZ-dependent synaptic NMDARs(Lau & Zukin, 2007). FRMPD2 is supposed as the potential PDZ protein to be capable of replenishing NMDAR-mediated excitatory synaptic transmission, providing a more comprehensive understanding of the roles of PDZ proteins in NMDAR targeting and function.

Our results showed that synaptic FRMPD2 mediated neurotransmission by trafficking GluN2A subunits on synapses in adult hippocampus. NMDA receptors are composed of obligatory GluN1 subunit co-assembled with GluN2A or GluN2B subunit (GluN1/GluN2A or GluN1/GluN2B). The identity of the GluN2A and/or GluN2B subunits determines the biophysical and pharmacological properties of NMDARs (Bard et al, 2010; Sultan et al, 2015). Our results of Co-IP, GST-pull-down and SPR assays identified the second PDZ domain of FRMPD2 as a novel binding partner of GluN2A *in vivo* and *in vitro*. Although the FRMPD2 PDZ2 did not directly bind to GluN1, the obligatory GluN1 subunit of GluN1/2A complex was, expectedly, detectable by Co-IP of FRMPD2. Meanwhile, the GluN1 protein of synaptosome was changed after FRMPD2 knockdown or overexpression, which was accompanied by the alteration of GluN2A subunits. It is interesting that the FRMPD2 did not pull down the GluN2B subunit *in vivo* or *in vitr*o. It might be because the binding of

PDZ2 to GluN2B is flexible and instant. In addition, only four amino acids were different between peptides sequences of C-termini of GluN2A and GluN2B in SPR experiments, the binding capacity of PDZ2 to GluN2A subunit was 1000 times higher than that to GluN2B subunit. It is probably that the GluN2B-containing NMDARs are located at extrasynaptic sites and involved in neurotoxicity in adult hippocampal neurons, GluN2A-containing NMDARs mainly resided at synaptic sites and involved in neurotransmission (Parsons et al, 2014). The low binding capacity of PDZ2 to GluN2B may partially explain that the FRMPD2 did not pull down the GluN2B subunit *in vivo* or *in vitr*o. Further investigation will be needed to explore that the binding of PDZ2 of FRMPD2 to GluN2A was stronger than that to GluN2B.

FRMPD2 was involved in excitatory synapses formation possibly in a Ferm domain-dependent manner. Ferm domain-containing proteins could function as a bridge between cytoskeletal structures and specific locations on the plasma membrane. The GST-Ferm domain of FRMPD2 was shown to bind to phosphatidylinositol PtdIns(3,4)P2, a key cofactor in signaling to the actin cytoskeleton(Stenzel et al, 2009). In our study, a direct interaction between the Ferm domain of FRMPD2 and F-actin was firstly reported. These data are consistent with previous reports showing that F-actin cosediments with other Ferm domain-containing proteins, including merlin and myo1(Gotesman et al, 2010; Sun et al, 2002). Ferm domain of FRMPD2 is capable of interacting with F-actin to link F-actin to the synaptic plasma membrane, especially the PSD, a growing ends of F-actin resulting in changes in the morphology of spines(Rao et al, 2000). Moreover,

the F-actin cytoskeleton plays a pivotal role in NMDAR trafficking(Lei et al, 2001), and dramatic increases in the proportion of NMDAR, especially GluN1/GluN2A subunits trafficking at the postsynaptic membrane can also efficiently facilitate dendritic spines maturation, which is tightly correlated with the strength of excitatory synapses in the hippocampus(Chen et al, 2011; Meyer et al, 2014).

In addition, although Ferm-containing proteins have been reported to bind to the C-terminal tail of metabotropic glutamate receptor 5 (mGluR5) by the Ferm domain (Hu et al, 2012b), in our study, the results of Co-IP and GST-pull-down assays did not reveal any interaction between the FRMPD2 Ferm domain and mGluR1 or mGluR5 (data not shown). The mechanisms underlying these interactions remain unclear.

Our study indicated that FRMPD2 increases susceptibility to epilepsy, probably by increasing the NMDARs, as well as excitatory synapses formation, which contribute to excitatory neurotransmission integratedly. Multiple characteristics associated with excitatory neurotransmission, from receptor trafficking to dendritic spine morphology, contribute to the etiology underlying epileptogenesis (Noebels, 2015). The NMDAR subunit GluN2A is powerfully implicated in the development of epilepsy, and mutations in the gene encoding GluN2A subunit cause idiopathic focal epilepsy (Endele et al, 2010; Lemke et al, 2013). Selectively blocking GluN2A-containing NMDARs impaired epileptogenesis in pilocarpine induced epileptic rat models (Chen et al, 2007), suggesting that the GluN2A subunit is a therapeutic target for epilepsy treatment. In addition, epileptic mice showed an increase in mature dendritic spines of excitatory neurons (Oberheim et al, 2008), and

disrupting of F-actin polymerization in dendritic spines induced epileptic seizures and a long-term increase in neuronal excitability (Sierra-Paredes et al, 2006).

In summary, the results presented here suggest a critical role of novel scaffold protein FRMPD2 in regulating NMDA receptors anchoring and dendritic spine maturation, both of which is critical for regulation of glutamatergic synapses transmission. The dysregulation of this scaffold protein contributed to the impaired excitatory conductance which has been associated with neurological disease epilepsy.

Methods and materials

DNA constructs

To make the Flag-tagged FRMPD2 expression constructs, the following human FRMPD2 sequences (uniprot: Q68DX3-1) were cloned into pcDNA3.1-3xFlag (Sigma): Flag-FRMPD2 (amino acids1-1309), Flag-ΔFerm (full length with a deletion at amino acids342-642), and Flag-Ferm (amino acids 342-642).

To construct the following GST fusion proteins, the PDZ or Ferm domain of mouse FRMPD2 (Uniprot: A0A140LI67) was subcloned into pGEX4T-1 with a GST tag: GST-PDZ1 (amino acids 786-872), GST-PDZ2 (amino acids 934-1027), GST-PDZ3 (amino acids 1071-1159) and GST-Ferm (amino acids 339-639).

The lentivirus vector (LV) constructs were manufactured by Genechem Co. Biotechnology (Shanghai City, China). The mouse FRMPD2 (NCBI Gene: 268729) short hairpin RNA (shRNA) knockdown construct targeted 5’-3’ CTGAATCTTTCTCTTGCAT and was subcloned it into the LV GV248 (GeneChem, China), which contained green fluorescent protein (GFP). A scramble shRNA (5’-3’ CTTTTCTAACGTGTCGACT) was used as a negative control for the FRMPD2 shRNA. The complete mouse cDNA sequence for FRMPD2 (XM_017316244) (FRMPD2 overexpression, FRMPD2 OE) and the GFP sequence were inserted into the LV GV358 (GeneChem, China).

Antibodies

The following antibodies were used: FRMPD2 (rabbit, Sigma;rabbit, Origene),

Flag(mouse, Sigma), GST(rabbit, Invitrogen), GFP (rabbit, Invitrogen), GluN2A(rabbit, Proteintech), GluN2B(mouse, Proteintech; rabbit, Abcam), GluN1(rabbit, Abcam), MAP2(guinea pig, SYSY), GFAP(mouse, Sigma), PSD-95(guinea pig, SYSY; mouse, Millipore), VGLUT1(guinea pig, SYSY), synaptophysin(rabbit, Abcam), syntaxin 1a(rabbit, Abcam).

Cell line cultures and transfection

HEK293T and SH-SY5Y cells were maintained in DMEM (Gibco) supplemented with 10% fetal bovine serum (Gibco), 100 U/mL penicillin and 100 μg/mL streptomycin (Gibco) at 37°C in 5% CO2. The cells were transfected with Flag-FRMPD2, Flag-Ferm or Flag- ΔFerm using Lipofectamine 2000 (Invitrogen)(Klein et al, 2017). At 4 h after transfection, the cells were rinsed with warm PBS and incubated in culture medium containing 10% fetal bovine serum.

Intrahippocampal injection of LV

Adult C57/BL6 male mice were obtained from the Experimental Animal Center of Chongqing Medical University. Intrahippocampal injection of LV was performed using a stereotaxic apparatus (Stoelting Co. Ltd Wood Dale, IL, USA). Briefly, the mice were anesthetized with pentobarbital (80mg/kg, intraperitoneal) and placed on stereotaxic apparatus. The reference points were bregma for the anterior-posterior axis, the midline for the medial-lateral axis and the dura mater for the dorsal-ventral axis with a tooth bar. LV particles were injected bilaterally into the

dorsal hippocampus through a glass pipette (0.2 μl/min) attached to a glass microsyringe(Shangguan et al, 2017). The mice were allowed to recover for 2 weeks after the vector injections.

Patch clamp recordings

Brain slices were prepared as previously reported(Chen et al, 2006; Kim et al, 2001). Briefly, C57/BL6 mice were anesthetized with pentobarbital. Brain slices (300 μm) were prepared with a Leica (Germany) VP1200S Vibratome and incubated in artificial cerebral spinal fluid (ACSF) (119 mM NaCl, 26 mM $NaHCO_3$, 2.5 mM KCl, 1 mM $MgCl_2$, 1.25 mM NaH_2PO_4, 2 mM $CaCl_2$ and 25 mM glucose, pH 7.4, 310 mOsm) bubbled with 5% CO_2 and 95% O_2 for at least 1 h at room temperature before recording. Whole-cell recording was performed as described previously(Liu et al, 2005). Glass microelectrodes (Sutter, USA) were shaped by a pipette puller (P-97, Sutter, USA) to a final resistance of 3–5 MΩ when the pipette was filled with internal solution. A multi-clamp 700B amplifier (Axon, USA) was used for the recordings. Signals were sampled at 10 kHz and filtered at 2 kHz. A stable baseline was obtained for at least 5 min prior to recording and data were discarded when the access resistance (15–20 MΩ) was changed by 20% at the end of recording. Mini Analysis 6.0.1 (Synaptosoft) and Clamp Fit 10.3 software (Axon) were used to analyze the recorded data.

For action potential (AP) recording, glass pipettes were filled with the following internal solution: 17.5 mM KCl, 0.5 mM EGTA, 122.5 Mm K-gluconate, 10 mM

HEPES, and 4 mM ATP, pH adjusted to 7.2 with KOH [20]. The internal solution used to record excitatory post-synaptic currents (EPSCs) contained: 17.5 mM CsCl, 10 mM HEPES, 4 mM ATP, 0.5 mM EGTA, 132.5 mM Cs-gluconate, and 5 mM QX-314. The internal solution used to record inhibitory post-synaptic currents (IPSCs) contained: 100 mM CsCl, 1 mM $MgCl_2$, 1 mM EGTA, 30 mM N-methyl-D-glucamine, 10 mM HEPES, 5 mM MgATP 0.5 mM Na_2GTP and 12 mM phosphocreatine.

Spontaneous activity was assessed by observing the neuron under current clamp for 1 min. Tetrodotoxin (TTX, 1 μM), bicuculline (10 μM), 6,7-dinitroquinoxaline-2,3(1H,4H)-dione (DNQX, 20 μM) and D-serine (10 μM) were added to Mg-free-ACSF to record NMDAR mEPSCs that held at −60 mV. TTX (1 μM), bicuculline (10 μM) and amino-5-phosphonopentanoate (AP-V, 40 μM) were added to ACSF to record AMPA mEPSCs. TTX(1 μM), DNQX(20 μM) and APV(40 μM) were added to ACSF to record mIPSCs that held at −70 mV (Shangguan et al, 2017).

Evoked EPSCs (eEPSCs) currents were generated with a 40μs pulse (0.1 Hz) from a stimulated isolation unit controlled by an AMPI generator (Master-8, USA). A bipolar stimulation electrode (FHC) was located ~100 μm rostral to the recording electrode in the same layer(Chen et al, 2008; Tang et al, 2015). The eEPSCs at −70 mV holding potential in the present of PTX (100 μM) was considered as the AMPAR-mediated current. Neurons were then held at +40 mV and the amplitude of the eEPSCs at 50 ms post-stimulus was interpreted as the NMDAR-mediated

current(Etherton et al, 2009; Etherton et al, 2011). Input-output curve of NMDAR eEPSCs were recorded in response to a series of stimulation intensities (pA). Paired-pulse ratio (PPR) recordings were voltage-clamped at +40 mV and obtained using a paired-pulse protocol of two stimuli at an inter-pulse interval of 50 ms. PPR values were defined as the ratio of the second peak amplitude to the first peak amplitude. The highly selective GluN2B subunit antagonist Ro25-6981 (Ro, 0.5μM) was applied to assess GluN2A-sensitive eEPSCs, and the selective GluN2A antagonist NVP-AAM077(NVP, 0.4μM) was added to record GluN2B component eEPSCs(Bartlett et al, 2007).

Western blotting

Samples boiled with 4X sample buffer at 95°C for 5 min, and then separated on 8-10% SDS-PAGE gels and transferred onto polyvinylidene difluoride membranes (Millipore). The target proteins were immunoblotted with primary antibodies overnight at 4°C and then incubated with HRP-conjugated secondary antibodies. The blots were imaged and quantified using a Fusion Imaging System. The quantitative densitometric values of the proteins were normalized to that of GAPDH or beta-actin.

Immunofluorescence

For animal tissues, brain were post-fixed at 4°C for 24 h. Floating slices (50 mm in thickness) were permeabilized with 0.5% Triton X-100 and blocked in goat serum. The slices were then incubated with primary antibodies overnight at 4°C followed by

incubation with secondary fluorescent conjugated antibodies at room temperature for 2 h. Images were captured using laser-scanning confocal microscopy (Nikon A1+R Microsystems) on an Olympus IX 70 inverted microscope (Olympus) equipped with a Fluoview FVX confocal scanning head. Areas of overlap and fluorescence intensity were analyzed using Image Pro Plus 6.0.

Sub-synaptic fractionation

Sub-synaptic fractionation was performed as previously described(Phillips et al, 2001). To obtain synaptosomes, adult mouse hippocampus were homogenized in solution buffer (0.32 M sucrose, 0.1 mM $CaCl_2$, 1 mM $MgCl_2$, 0.1 mM PMSF) and brought to a final sucrose concentration of 1.25 M. Protease inhibitors were used in all purification steps. The homogenate was overlaid with 1.0 M sucrose and centrifuged (100,000 g, 3 h, 4°C). Synaptosomes were collected at the 1 M/1.25 M interface.

For sub-synaptic fractionation, synaptosomes were sequentially extracted with 1% Triton X-100 first at pH 6.0 and then at pH 8.0. Synaptosomes (described above) were diluted 1:10 with 0.1 mM $CaCl_2$ to a final concentration of 20 mM Tris, pH 6.0 and 1% Triton X-100. After the solution was incubated for 30 min and then centrifuged 40,000 g for 30 min at 4°C. The supernatant (presynaptic fraction) were precipitated with 10 volumes of acetone at −20°C and recovered by centrifugation (20,000 g; 30 min, 4°C). The pellet containing insoluble postsynaptic density (PSD) was resuspended in 10 volumes solution buffer (1% Triton X-100, 20 μM Tris, pH

8.0, 4°C), incubated for 30 min, and centrifuged (40,000 g, 30 min, 4°C).

GST-pull-down and co-immunoprecipitation assays.

The methods used to produce the GST fusion proteins in bacteria have been previously reported (Anzai et al, 2002; Anzai et al, 2004). GST-pull-down assays were carried out using a GST Protein Interaction Pull-Down Kit (Pierce) according to the manufacturer's instructions. Briefly, the bacterial lysate containing the fusion proteins was sonicated and centrifuged, and the supernatant was used for protein binding assays. In vitro translation was facilitated using a plasmid carrying full-length GluN2A, GluN2B or GluN1 (Addgene) that was transfected into HEK293T cells. The translated total proteins obtained from cells and the GST fusion proteins were incubated together with GST glutathione agarose resin. The protein complexes were then eluted by glutathione and analyzed by Western blotting using GST, GFP, GluN2A, GluN2B or GluN1 antibodies.

For co-immunoprecipitation assays, the extracts contained in the crude synaptosomal fraction obtained from adult mouse hippocampal tissues were prepared with anti-GluN2A, anti-GluN2B, anti-GluN1 or anti-FRMPD2 antibodies or IgG (rabbit, Abcam) (Control) at 4°C for 12 h before they were incubated with protein A/G agarose beads (Beyotime). The immunoprecipitated mixture was immunoblotted with GluN2A, GluN2B, GluN1 or FRMPD2 antibodies.

Golgi staining

Golgi staining was performed using a Hito Golgi-Cox OptimStain Kit according to the manufacturer's protocol (Hitobiotec Inc.). Spines were counted on secondary and tertiary branches of apical and basal dendrites in the CA1 hippocampal. 5 neurons were chosen from 3 mice per group, and 5 counting segments (10 μm in length) of either secondary or tertiary dendrites were randomly selected from each neuron for statistical comparison. Dendrite length was measured using Image pro plus 6.0.

Actin cosedimentation assays.

F-actin binding assays were performed as described by the manufacturer (Cytoskeleton). Briefly, α-actinin and purified GST-Ferm (amino acids 339-639) of mouse FRMPD2 were incubated with freshly polymerized actin (F-actin) for 30 min at room temperature, and then subjected to ultracentrifugation (150,000 x g) for 1.5 h to pellet the proteins that had bound to F-actin. The pellet and supernatant were analyzed by Coomassie blue staining.

Surface Plasmon Resonance (SPR) assays.

SPR biosensor analysis was used to verify binding between peptides and the PDZ2 domain of FRMPD2 protein using a Biacore 8K instrument (GE Healthcare), as previously described(Zhang et al, 2014a). Proteins were immobilized on S CM5 chips using amine-coupling chemistry. Binding experiments were performed in running buffer (10 mM PBS, pH 7, 0.05% P20) at 25°C with a flow rate of 30 μL/min.

Gradient concentrations of PDZ2 proteins were diluted to 50 ug/ml in sodium acetate(10 mM, pH 5.5) and injected into the channel for 120 s, followed by disassociation for 120 s. RU values were collected at 10 Hz and all the experimental data were globally analyzed in a steady-state model within Biacore 8K Evaluation software.

Transmission electron microscopy

Tissues were prepared and sectioned for transmission electron microcscopy as previously described(Hu et al, 2012a). Briefly, mice were transcardially perfused with 2.5% glutaraldehyde and 4% paraformaldehyde. Brain tissue (1 mm^3 size) was cut from the hippocampus CA1 area, fixed in 2.5% glutaraldehyde for 2 h, post-fixed in 1% osmium tetroxide for 2 h and then dehydrated through ethanol gradients. After the tissues were embedded in Epon 618 epoxy resin, the samples were cut into ultrathin sections by an ultramicrotome (LKB-V, LKB Produkter AB, Sweden), and double-stained by uranyl acetate/lead citrate. Ultra-structures were observed by transmission electron microscope (JEM-1400PLUS, JEOL, Japan). In the present study, excitatory synapses were identified as those with round vesicles and asymmetric pre- and postsynaptic dense material, while inhibitory synapses were identified as those with flattened vesicles and symmetric dense material(Larramendi et al, 1967; Weeks et al, 2007). Sampling fields were randomly selected for imaging in each section, and measured using the software Image Pro Plus 6.0.

Human samples

Temporal lobe tissues were randomly obtained from twenty post-surgery patients treated for TLE for whom tissues were available in our brain tissue bank (Shangguan et al, 2017; Xu et al, 2017; Zhang et al, 2014b). A diagnosis of TLE was determined based on the 2001 International Classification of Epileptic Seizures by the International League Against Epilepsy (ILAE)(Engel, 2001). The temporal cortical tissues used as control samples were obtained from twelve randomized patients who underwent surgery for trauma-induced intracranial hypertension. The control patients had no history of epilepsy, no exposure to antiepileptic drugs, and no history of neurological or psychiatric disorders. A neuropathological examination confirmed that the temporal neocortex specimens obtained from the control patients were normal. There was no significant difference in age or gender between the TLE and control patients (Supplementary Table 2).

Animal behaviors in epilepsy

Two weeks after the intrahippocampal injection of LV, the mice were kindled by pentylenetetrazol (PTZ) or kainic acid (KA) to measure epilepsy susceptibility. This PTZ induced model was performed according to the methods described in a previously study(Gelfuso et al, 2013). C57/BL6 mice were administered an intraperitoneal injection of PTZ (35 mg/kg) every other day and then observed for 60 min after each injection. Behavioral seizure scores were assessed based on the Racine standard scale, as follows: Grade 0 indicated arrest, wet dog shaking, and normal

behavior; Grade 1 indicated facial twitches (nose, lips, and eyes); Grade 2 indicated chewing and head nodding; Grade 3 indicated forelimb clonus; Grade 4 indicated rearing and falling on forelimbs; and Grade 5 indicated imbalance and falling on the side or back(Racine, 1972). Only fully induced seizures (Grades 4 and 5) were evaluated to determine the number of seizures and the latency period. The controls was not performed at least 3 consecutive seizures with a score of 4 or 5.

Mice were injected with KA as previously described (Bitsika et al, 2016). Briefly, two weeks after the intrahippocampal injection of LV, the mice were anesthetized and slowly injected with KA (1 nmol in 50 nl) into dorsal hippocampus via a guide cannula under stereotaxic guidance. At one hour after the onset of KA-induced status epilepticus(SE), diazepam (10 mg/kg, i.p.) was administered to suppress SE. Then, the animals were video recorded for twenty-four hours to monitor spontaneous recurrent seizures (SRSs) for 1 month. Seizure scores were evaluated on the Racine scale (see above), and only seizures with a score of 4 or 5 were recorded to determine the number of SRSs and the latency period that between the SE termination and the first SRS. Multichannel electroencephalogram (EEG) recording was performed to quantify the EEG seizures using the OmniPlex® D Neuronal Data Acquisition System (Plexon, Dallas, TX) as previously described(Shangguan et al, 2017; Xu et al, 2017). The signals were preamplified (1000×), filtered (0.1-1000 Hz), and digitized at 4 kHz. EEG seizures like events were characterized by high frequencies (>5 Hz), high amplitudes (>2 times the baseline), and durations of >5 s (Jimenez-Mateos et al, 2012).

Study approval

All protocols of animal studies were approved by the Commission of Chongqing Medical University for the ethics of experiments on animals and conducted in accordance with international standards. All procedures of human samples collections were formally consented to by the patients or their lineal relatives and approved by the Ethics Committee of Chongqing Medical University according to the tenets of the Declaration of Helsinki.

Statistical analysis

All averaged data are presented as the means ± SD, and all graphs were prepared using GraphPad Prism 4 software (La Jolla, CA). For independent-samples, Student's t-test was used. Repeated measures ANOVA followed by post hoc t-tests was used to measure differences between two groups at multiple time points. The $\chi 2$ test was used to compare gender differences between the patients in the TLE and control groups. $p<0.05$ and 0.01 were considered to indicate statistical significance and are indicated as $*p<0.05$ or $**p<0.01$, respectively. All tests were two-sided. n indicates the number of cells/slices or independent experiments and was used to calculate the degree of freedom. All samples included in each experiment were analyzed in triplicate.

Acknowledgements

The authors are sincerely grateful for the support of Beijing Tiantan Hospital, Beijing Xuanwu Hospital, and the Daping Hospital of the Third Military Medical University for supplying the brain tissues used in this study. In addition, we thank all of the patients and their families for their participation in this study. This work was supported by grants from the National Natural Science Foundation of China (No. 81271445, 81471319, 81301109, and 81301110) and the National Clinical Key Specialty Construction Foundation of China.

Author contributions

X. L. and XF. W. conceived and designed the experiments. HQ. Z., Y.L., RJ.Z., MQ.H. and YL. M. performed the experiments. X. L. collected and analyzed the data. X. L. wrote the manuscript. All authors contributed to preparation of the paper and approved the final contributions.

The authors have declared that no conflict of interest exists.

References

Adams PD, Afonine PV, Bunkoczi G, Chen VB, Davis IW, Echols N, Headd JJ, Hung LW, Kapral GJ, Grosse-Kunstleve RW, McCoy AJ, Moriarty NW, Oeffner R, Read RJ, Richardson DC, Richardson JS, Terwilliger TC, Zwart PH (2010) PHENIX: a comprehensive Python-based system for macromolecular structure solution. *Acta crystallographica Section D, Biological crystallography* **66:** 213-221

Anzai N, Deval E, Schaefer L, Friend V, Lazdunski M, Lingueglia E (2002) The multivalent PDZ domain-containing protein CIPP is a partner of acid-sensing ion channel 3 in sensory neurons. *The Journal of biological chemistry* **277:** 16655-16661

Anzai N, Miyazaki H, Noshiro R, Khamdang S, Chairoungdua A, Shin HJ, Enomoto A, Sakamoto S, Hirata T, Tomita K, Kanai Y, Endou H (2004) The multivalent PDZ domain-containing protein PDZK1 regulates transport activity of renal urate-anion exchanger URAT1 via its C terminus. *The Journal of biological chemistry* **279:** 45942-45950

Bard L, Sainlos M, Bouchet D, Cousins S, Mikasova L, Breillat C, Stephenson FA, Imperiali B, Choquet D, Groc L (2010) Dynamic and specific interaction between synaptic NR2-NMDA receptor and PDZ proteins. *Proceedings of the National Academy of Sciences of the United States of America* **107:** 19561-19566

Bartlett TE, Bannister NJ, Collett VJ, Dargan SL, Massey PV, Bortolotto ZA, Fitzjohn SM, Bashir ZI, Collingridge GL, Lodge D (2007) Differential roles of NR2A and NR2B-containing NMDA receptors in LTP and LTD in the CA1 region of two-week old rat hippocampus. *Neuropharmacology* **52:** 60-70

Beique JC, Andrade R (2003) PSD-95 regulates synaptic transmission and plasticity in rat cerebral cortex. *The Journal of physiology* **546:** 859-867

Beique JC, Lin DT, Kang MG, Aizawa H, Takamiya K, Huganir RL (2006) Synapse-specific regulation of AMPA receptor function by PSD-95. *Proceedings of the National Academy of Sciences of the United States of America* **103:** 19535-19540

Bitsika V, Duveau V, Simon-Areces J, Mullen W, Roucard C, Makridakis M, Mermelekas G, Savvopoulos P, Depaulis A, Vlahou A (2016) High-Throughput LC-MS/MS Proteomic Analysis of a Mouse Model of Mesiotemporal Lobe Epilepsy Predicts Microglial Activation Underlying Disease Development. *Journal of proteome research* **15:** 1546-1562

Bourne JN, Harris KM (2008) Balancing structure and function at hippocampal dendritic spines. *Annual review of neuroscience* **31:** 47-67

Bredt DS, Nicoll RA (2003) AMPA receptor trafficking at excitatory synapses. *Neuron* **40:** 361-379

Chen BS, Thomas EV, Sanz-Clemente A, Roche KW (2011) NMDA receptor-dependent regulation of dendritic spine morphology by SAP102 splice variants. *The Journal of neuroscience : the official*

696 *journal of the Society for Neuroscience* **31:** 89-96
697
698 Chen G, Chen P, Tan H, Ma D, Dou F, Feng J, Yan Z (2008) Regulation of the NMDA receptor-mediated
699 synaptic response by acetylcholinesterase inhibitors and its impairment in an animal model of
700 Alzheimer's disease. *Neurobiology of aging* **29:** 1795-1804
701
702 Chen G, Kittler JT, Moss SJ, Yan Z (2006) Dopamine D3 receptors regulate GABAA receptor function
703 through a phospho-dependent endocytosis mechanism in nucleus accumbens. *The Journal of*
704 *neuroscience : the official journal of the Society for Neuroscience* **26:** 2513-2521
705
706 Chen Q, He S, Hu XL, Yu J, Zhou Y, Zheng J, Zhang S, Zhang C, Duan WH, Xiong ZQ (2007) Differential
707 roles of NR2A- and NR2B-containing NMDA receptors in activity-dependent brain-derived
708 neurotrophic factor gene regulation and limbic epileptogenesis. *The Journal of neuroscience : the*
709 *official journal of the Society for Neuroscience* **27:** 542-552
710
711 Durand CM, Perroy J, Loll F, Perrais D, Fagni L, Bourgeron T, Montcouquiol M, Sans N (2012) SHANK3
712 mutations identified in autism lead to modification of dendritic spine morphology via an
713 actin-dependent mechanism. *Molecular psychiatry* **17:** 71-84
714
715 Elias GM, Elias LA, Apostolides PF, Kriegstein AR, Nicoll RA (2008) Differential trafficking of AMPA and
716 NMDA receptors by SAP102 and PSD-95 underlies synapse development. *Proceedings of the National*
717 *Academy of Sciences of the United States of America* **105:** 20953-20958
718
719 Elias GM, Funke L, Stein V, Grant SG, Bredt DS, Nicoll RA (2006) Synapse-specific and developmentally
720 regulated targeting of AMPA receptors by a family of MAGUK scaffolding proteins. *Neuron* **52:**
721 307-320
722
723 Elias GM, Nicoll RA (2007) Synaptic trafficking of glutamate receptors by MAGUK scaffolding proteins.
724 *Trends in cell biology* **17:** 343-352
725
726 Endele S, Rosenberger G, Geider K, Popp B, Tamer C, Stefanova I, Milh M, Kortum F, Fritsch A, Pientka
727 FK, Hellenbroich Y, Kalscheuer VM, Kohlhase J, Moog U, Rappold G, Rauch A, Ropers HH, von Spiczak S,
728 Tonnies H, Villeneuve N et al (2010) Mutations in GRIN2A and GRIN2B encoding regulatory subunits
729 of NMDA receptors cause variable neurodevelopmental phenotypes. *Nature genetics* **42:** 1021-1026
730
731 Engel J, Jr. (2001) Intractable epilepsy: definition and neurobiology. *Epilepsia* **42 Suppl 6:** 3
732
733 Etherton MR, Blaiss CA, Powell CM, Sudhof TC (2009) Mouse neurexin-1alpha deletion causes
734 correlated electrophysiological and behavioral changes consistent with cognitive impairments.
735 *Proceedings of the National Academy of Sciences of the United States of America* **106:** 17998-18003
736
737 Etherton MR, Tabuchi K, Sharma M, Ko J, Sudhof TC (2011) An autism-associated point mutation in
738 the neuroligin cytoplasmic tail selectively impairs AMPA receptor-mediated synaptic transmission in
739 hippocampus. *The EMBO journal* **30:** 2908-2919

740
741 Feng W, Zhang M (2009) Organization and dynamics of PDZ-domain-related supramodules in the
742 postsynaptic density. *Nature reviews Neuroscience* **10:** 87-99
743
744 Gelfuso EA, Liberato JL, Cunha AO, Mortari MR, Beleboni RO, Lopes NP, Dos Santos WF (2013)
745 Parawixin2, a novel non-selective GABA uptake inhibitor from Parawixia bistriata spider venom,
746 inhibits pentylenetetrazole-induced chemical kindling in rats. *Neuroscience letters* **543:** 12-16
747
748 Gianni S, Walma T, Arcovito A, Calosci N, Bellelli A, Engstrom A, Travaglini-Allocatelli C, Brunori M,
749 Jemth P, Vuister GW (2006) Demonstration of long-range interactions in a PDZ domain by NMR,
750 kinetics, and protein engineering. *Structure (London, England : 1993)* **14:** 1801-1809
751
752 Gotesman M, Hosein RE, Gavin RH (2010) A FERM domain in a class XIV myosin interacts with actin
753 and tubulin and localizes to the cytoskeleton, phagosomes, and nucleus in Tetrahymena thermophila.
754 *Cytoskeleton (Hoboken, NJ)* **67:** 90-101
755
756 Harris KM, Weinberg RJ (2012) Ultrastructure of synapses in the mammalian brain. *Cold Spring Harbor*
757 *perspectives in biology* **4**
758
759 Hruska-Hageman AM, Wemmie JA, Price MP, Welsh MJ (2002) Interaction of the synaptic protein
760 PICK1 (protein interacting with C kinase 1) with the non-voltage gated sodium channels BNC1 (brain
761 Na+ channel 1) and ASIC (acid-sensing ion channel). *The Biochemical journal* **361:** 443-450
762
763 Hu B, Chen H, Yang L, Tao ZF, Yan J, Zhang YH, Zhu ZR, Sun WZ, Huang W, Huang WQ, Sui JF (2012a)
764 Changes of synaptic ultrastructure in the guinea pig interpositus nuclei associate with response
765 magnitude and timing after trace eyeblink conditioning. *Behavioural brain research* **226:** 529-537
766
767 Hu JH, Yang L, Kammermeier PJ, Moore CG, Brakeman PR, Tu J, Yu S, Petralia RS, Li Z, Zhang PW, Park
768 JM, Dong X, Xiao B, Worley PF (2012b) Preso1 dynamically regulates group I metabotropic glutamate
769 receptors. *Nature neuroscience* **15:** 836-844
770
771 Jimenez-Mateos EM, Engel T, Merino-Serrais P, McKiernan RC, Tanaka K, Mouri G, Sano T, O'Tuathaigh
772 C, Waddington JL, Prenter S, Delanty N, Farrell MA, O'Brien DF, Conroy RM, Stallings RL, DeFelipe J,
773 Henshall DC (2012) Silencing microRNA-134 produces neuroprotective and prolonged
774 seizure-suppressive effects. *Nature medicine* **18:** 1087-1094
775
776 Kim CH, Chung HJ, Lee HK, Huganir RL (2001) Interaction of the AMPA receptor subunit GluR2/3 with
777 PDZ domains regulates hippocampal long-term depression. *Proceedings of the National Academy of*
778 *Sciences of the United States of America* **98:** 11725-11730
779
780 Kim E, Sheng M (2004) PDZ domain proteins of synapses. *Nature reviews Neuroscience* **5:** 771-781
781
782 Klein ZA, Takahashi H, Ma M, Stagi M, Zhou M, Lam TT, Strittmatter SM (2017) Loss of TMEM106B
783 Ameliorates Lysosomal and Frontotemporal Dementia-Related Phenotypes in Progranulin-Deficient

Mice. *Neuron* **95:** 281-296.e286

Kwan P, Schachter SC, Brodie MJ (2011) Drug-resistant epilepsy. *The New England journal of medicine* **365:** 919-926

Larramendi LM, Fickenscher L, Lemkey-Johnston N (1967) Synaptic vesicles of inhibitory and excitatory TERMINALS IN THE CEREBELLUM. *Science (New York, NY)* **156:** 967-969

Lau CG, Zukin RS (2007) NMDA receptor trafficking in synaptic plasticity and neuropsychiatric disorders. *Nature reviews Neuroscience* **8:** 413-426

Lee SE, Kim Y, Han JK, Park H, Lee U, Na M, Jeong S, Chung C (2016) nArgBP2 regulates excitatory synapse formation by controlling dendritic spine morphology. **113:** 6749-6754

Lei S, Czerwinska E, Czerwinski W, Walsh MP, MacDonald JF (2001) Regulation of NMDA receptor activity by F-actin and myosin light chain kinase. *The Journal of neuroscience : the official journal of the Society for Neuroscience* **21:** 8464-8472

Lemke JR, Lal D, Reinthaler EM, Steiner I, Nothnagel M, Alber M, Geider K, Laube B, Schwake M, Finsterwalder K, Franke A, Schilhabel M, Jahn JA, Muhle H, Boor R, Van Paesschen W, Caraballo R, Fejerman N, Weckhuysen S, De Jonghe P et al (2013) Mutations in GRIN2A cause idiopathic focal epilepsy with rolandic spikes. *Nature genetics* **45:** 1067-1072

Lipinski S, Grabe N, Jacobs G, Billmann-Born S, Till A, Hasler R, Aden K, Paulsen M, Arlt A, Kraemer L, Hagemann N, Erdmann KS, Schreiber S, Rosenstiel P (2012) RNAi screening identifies mediators of NOD2 signaling: implications for spatial specificity of MDP recognition. *Proceedings of the National Academy of Sciences of the United States of America* **109:** 21426-21431

Liu QS, Pu L, Poo MM (2005) Repeated cocaine exposure in vivo facilitates LTP induction in midbrain dopamine neurons. *Nature* **437:** 1027-1031

Meyer D, Bonhoeffer T, Scheuss V (2014) Balance and stability of synaptic structures during synaptic plasticity. *Neuron* **82:** 430-443

Noebels J (2015) Pathway-driven discovery of epilepsy genes. *Nature neuroscience* **18:** 344-350

Oberheim NA, Tian GF, Han X, Peng W, Takano T, Ransom B, Nedergaard M (2008) Loss of astrocytic domain organization in the epileptic brain. *The Journal of neuroscience : the official journal of the Society for Neuroscience* **28:** 3264-3276

Parsons MP, Raymond LA (2014) Extrasynaptic NMDA receptor involvement in central nervous system disorders. *Neuron* **82:** 279-293

Phillips GR, Huang JK, Wang Y, Tanaka H, Shapiro L, Zhang W, Shan WS, Arndt K, Frank M, Gordon RE,

828 Gawinowicz MA, Zhao Y, Colman DR (2001) The presynaptic particle web: ultrastructure, composition,
829 dissolution, and reconstitution. *Neuron* **32:** 63-77
830
831 Racine RJ (1972) Modification of seizure activity by electrical stimulation. II. Motor seizure.
832 *Electroencephalography and clinical neurophysiology* **32:** 281-294
833
834 Rao A, Craig AM (2000) Signaling between the actin cytoskeleton and the postsynaptic density of
835 dendritic spines. *Hippocampus* **10:** 527-541
836
837 Sala C, Piech V, Wilson NR, Passafaro M, Liu G, Sheng M (2001) Regulation of dendritic spine
838 morphology and synaptic function by Shank and Homer. *Neuron* **31:** 115-130
839
840 Schultz J, Hoffmuller U, Krause G, Ashurst J, Macias MJ, Schmieder P, Schneider-Mergener J, Oschkinat
841 H (1998) Specific interactions between the syntrophin PDZ domain and voltage-gated sodium
842 channels. *Nature structural biology* **5:** 19-24
843
844 Shangguan Y, Xu X, Ganbat B, Li Y, Wang W, Yang Y, Lu X, Du C, Tian X, Wang X (2017) CNTNAP4
845 Impacts Epilepsy Through GABAA Receptors Regulation: Evidence From Temporal Lobe Epilepsy
846 Patients and Mouse Models. *Cerebral cortex (New York, NY : 1991)***:** 1-14
847
848 Shen G, Van Sickle BJ, Tietz EI (2010) Calcium/calmodulin-dependent protein kinase II mediates
849 hippocampal glutamatergic plasticity during benzodiazepine withdrawal. *Neuropsychopharmacology :*
850 *official publication of the American College of Neuropsychopharmacology* **35:** 1897-1909
851
852 Sheng M, Hoogenraad CC (2007) The postsynaptic architecture of excitatory synapses: a more
853 quantitative view. *Annual review of biochemistry* **76:** 823-847
854
855 Sierra-Paredes G, Oreiro-Garcia T, Nunez-Rodriguez A, Vazquez-Lopez A, Sierra-Marcuno G (2006)
856 Seizures induced by in vivo latrunculin a and jasplakinolide microperfusion in the rat hippocampus.
857 *Journal of molecular neuroscience : MN* **28:** 151-160
858
859 Stenzel N, Fetzer CP, Heumann R, Erdmann KS (2009) PDZ-domain-directed basolateral targeting of
860 the peripheral membrane protein FRMPD2 in epithelial cells. *Journal of cell science* **122:** 3374-3384
861
862 Sultan S, Li L, Moss J, Petrelli F, Casse F, Gebara E, Lopatar J, Pfrieger FW, Bezzi P, Bischofberger J, Toni
863 N (2015) Synaptic Integration of Adult-Born Hippocampal Neurons Is Locally Controlled by Astrocytes.
864 *Neuron* **88:** 957-972
865
866 Sun CX, Robb VA, Gutmann DH (2002) Protein 4.1 tumor suppressors: getting a FERM grip on growth
867 regulation. *Journal of cell science* **115:** 3991-4000
868
869 Tang B, Luo D, Yang J, Xu XY, Zhu BL, Wang XF, Yan Z, Chen GJ (2015) Modulation of AMPA receptor
870 mediated current by nicotinic acetylcholine receptor in layer I neurons of rat prefrontal cortex.
871 *Scientific reports* **5:** 14099

Valtschanoff JG, Weinberg RJ (2001) Laminar organization of the NMDA receptor complex within the postsynaptic density. *The Journal of neuroscience : the official journal of the Society for Neuroscience* **21:** 1211-1217

Weeks AC, Connor S, Hinchcliff R, LeBoutillier JC, Thompson RF, Petit TL (2007) Eye-blink conditioning is associated with changes in synaptic ultrastructure in the rabbit interpositus nuclei. *Learning & memory (Cold Spring Harbor, NY)* **14:** 385-389

Xu X, Shangguan Y, Lu S, Wang W (2017) Tubulin beta-III modulates seizure activity in epilepsy. **242:** 297-308

Yang Y, Baboolal TG, Siththanandan V, Chen M, Walker ML, Knight PJ, Peckham M, Sellers JR (2009) A FERM domain autoregulates Drosophila myosin 7a activity. *Proceedings of the National Academy of Sciences of the United States of America* **106:** 4189-4194

Zhang C, Wan X, Zheng X, Shao X, Liu Q, Zhang Q, Qian Y (2014a) Dual-functional nanoparticles targeting amyloid plaques in the brains of Alzheimer's disease mice. *Biomaterials* **35:** 456-465

Zhang X, Chen G, Lu Y, Liu J, Fang M, Luo J, Cao Q, Wang X (2014b) Association of mitochondrial letm1 with epileptic seizures. *Cerebral cortex (New York, NY : 1991)* **24:** 2533-2540

Zucker RS, Regehr WG (2002) Short-term synaptic plasticity. *Annual review of physiology* **64:** 355-405

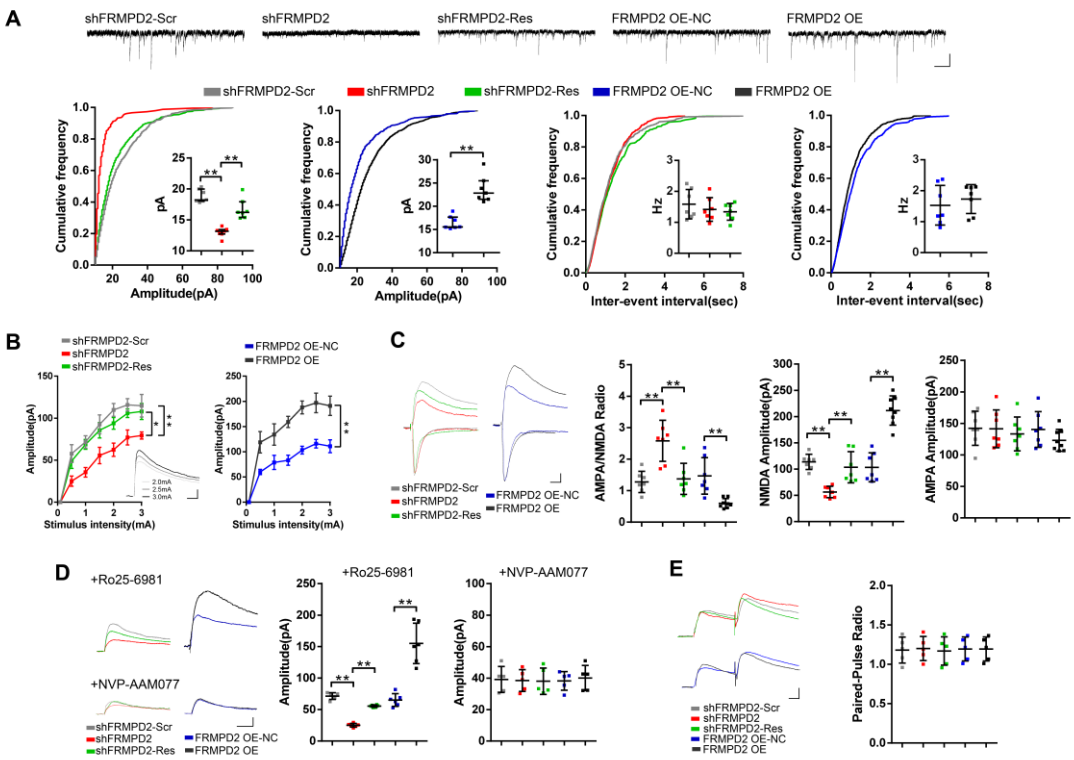

Fig 1. Effects of FRMPD2 on NMDA receptor-mediated excitatory synaptic transmission.

A, Quantitative analysis of amplitude and frequency of NMDAR mEPSCs in CA1 pyramidal cells of hippocampus after FRMPD2 knockdown or overexpression. Bar, 1 s, 20 pA. B, The input-output curves of NMDAR eEPSCs were recorded with gradual increasing intensities. Bar, 25 ms, 50 pA. C, Amplitude of NMDAR, AMPAR component eEPSCs and AMPA/NMDA ratio were compared. Bar, 25 ms, 25 pA. D, Quantitative analysis of the amplitude of GluN2A- and GluN2B-sensitive eEPSCs. Bar, 25 ms, 25 pA. E, Knocking down or overexpressing FRMPD2 did not alter the paired-pulse ratio (PPR) values. Bar, 25 ms, 50 pA. Data of were presented as the mean±SD or median with interquartile range. Data of A, C, D, E, were analyzed by Student's *t* test, data of B was analyzed by repeated measures ANOVA, n=5-7 neurons from 3 mice. **p<0.01. *p<0.05.

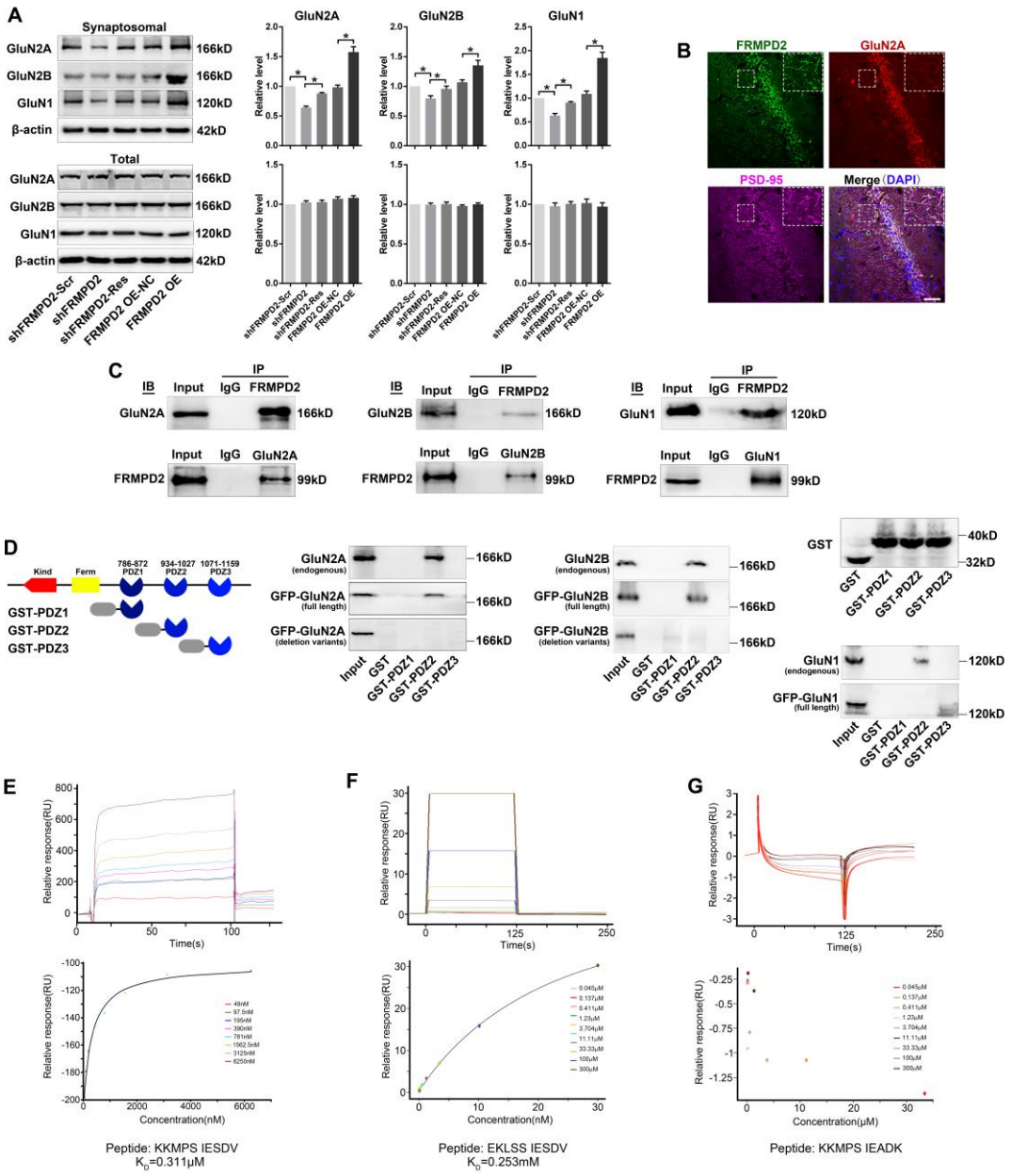

Fig 2. Effects of FRMPD2 anchoring GluN2A at synapses.

A, Quantitative analysis of GluN2A, GluN2B and GluN1 expressions of total hippocampus tissue and synaptic homogenates after FRMPD2 knockdown or overexpression. The data were shown as the mean±SD and analyzed by Student's *t* test, *p< 0.05. B, Immunofluorescence staining in the mouse hippocampus CA1 area showed that FRMPD2 co-localizes with GluN2A at the postsynaptic density, which was marked by PSD95. Bar, 40 μm. C, FRMPD2 and GluN2A, GluN2B and GluN1

were co-immunoprecipitated from mouse hippocampal tissues. D, GST pull-down assay showing that the GST-PDZ2 fusion protein but not the PDZ1 or PDZ3 fusion proteins pulled down endogenous GluN2A from mouse hippocampal tissues, and exogenous full-length GFP-GluN2A from HEK293 cells but did not pull down the deletion variant GFP-GluN2A from HEK293 cells transfected with GFP-GluN2A that lacked ten amino acids at the C-terminus. E-G, The ability of the isolated FRMPD2 PDZ2 domain to bind to the GluN2A and GluN2B C-terminus was measured using SPR. Peptides sequences of C-termini of wild type GluN2A (E), wild type GluN2B (F) and mutant GluN2A (G) were used in this study. Sensorgrams were shown to illustrate the binding of increasing concentrations of the PDZ2 domain to peptides and steady-state equilibrium responses from the sensorgrams were shown plotted against the injected PDZ2 concentrations. K_D: dissociation constant.

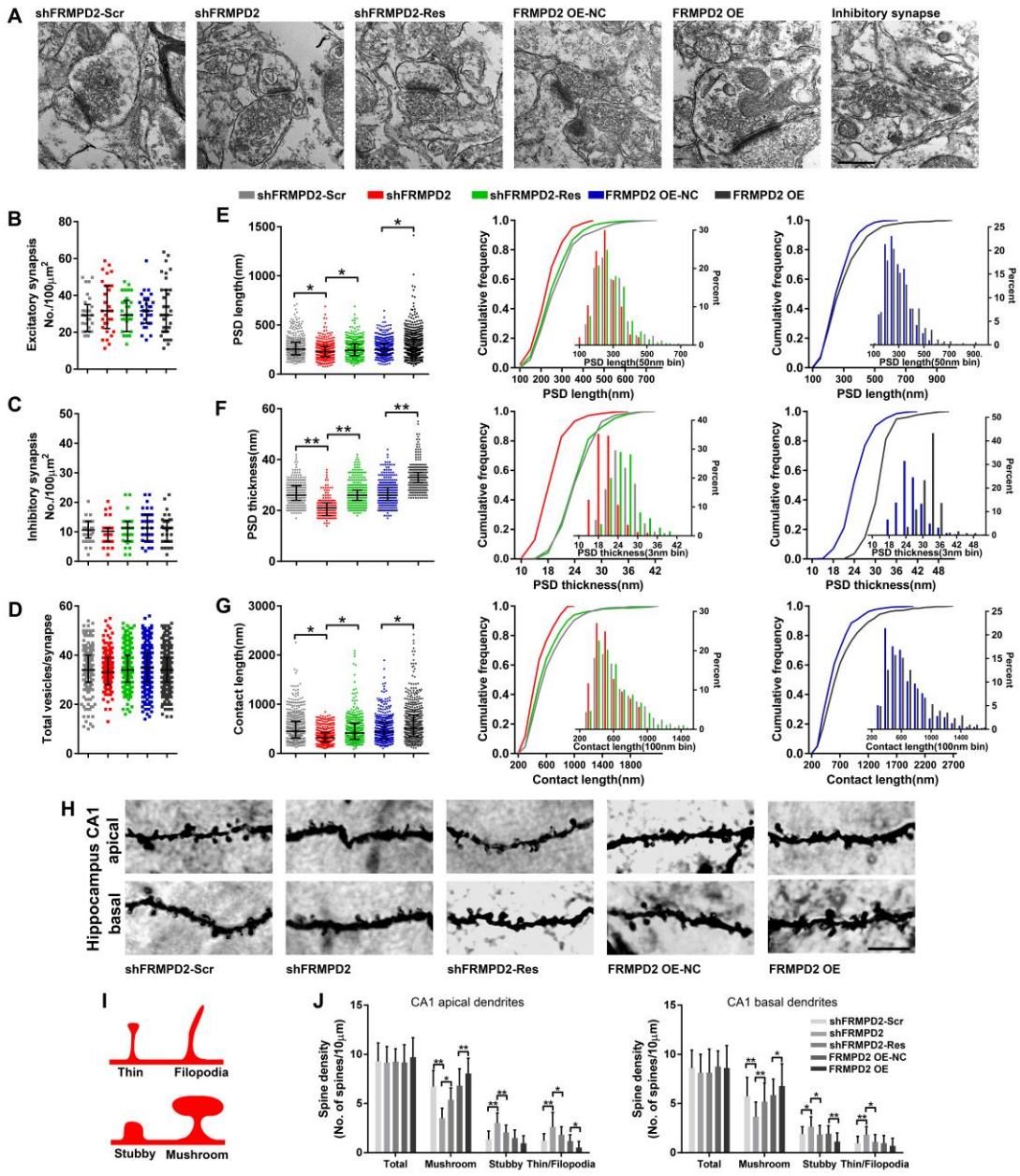

Fig 3. Effects of FRMPD2 on the formation of excitatory synapses in hippocampus CA1 area.

A, Electron micrograph of a spine synapse showing a typical continuous electron dense PSD and contact length. Scale bar, 400 nm; n=10-12 images from 3 mice. B-D, The number of excitatory synapses(B), inhibitory synapse(C) and vesicles per synapse(D) were compared after FRMPD2 knockdown or overexpression. E-F, Quantitative analysis and distribution of PSD length (E) and thickness (F) were

shown. G, Quantitative analysis and distribution of contacted length of the spine with the presynaptic terminal were represented. H, Representative images of Golgi staining to showed spine morphology in basal and apical dendrites of CA1 hippocampal neurons. Bar, 10 μm. I, Illustration of different spine morphologies: mushroom, thin, stubby, and filopodia. J, Quantification analysis showed the densities of total, mature and immature spines in both the apical and basal dendrites of CA1 hippocampal neurons in the FRMPD2 knockdown or overexpression mice. The data were shown as the mean±SD or median with interquartile range; *$p < 0.05$, **$p < 0.01$.

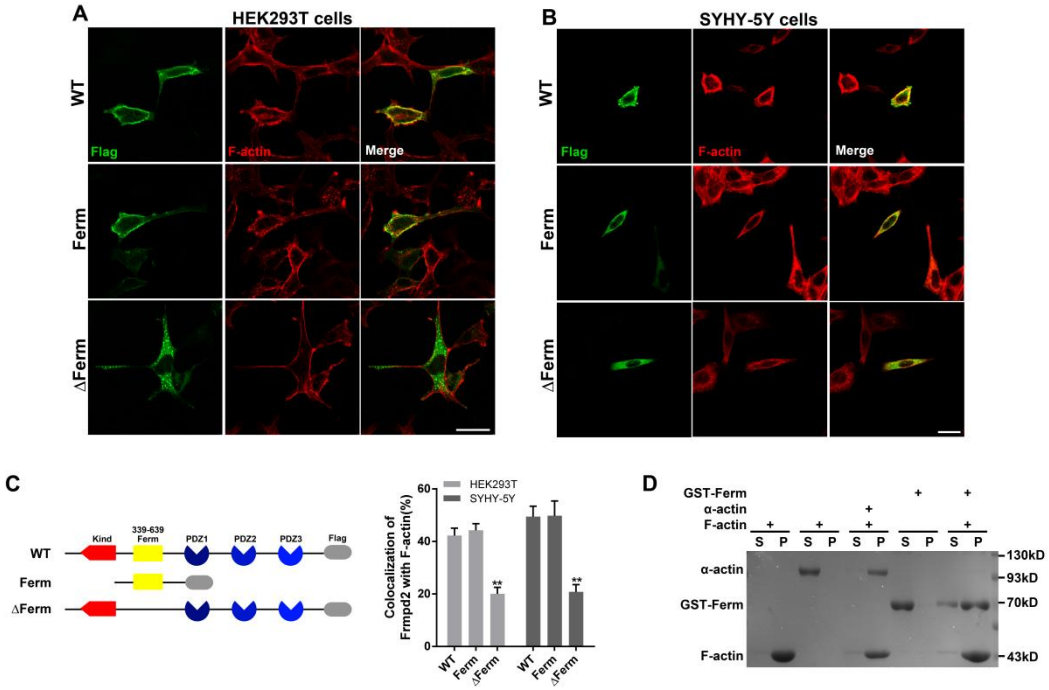

Fig 4. Binding of the FRMPD2 Ferm domain with F-actin.

A, B, The Ferm domain of FRMPD2 was sufficient and required for F-actin colocalization. HEK293 (A) and SYHY-5Y (B) cells were transfected with Flag-tagged FRMPD2 (WT), a deletion variants (ΔFerm) or only the Ferm domain (Ferm) and then stained for Flag and F-actin (rhodamine-phalloidin). Scale bar, 50 μm. C, Quantification of colocalization in FRMPD2 variants between Flag and F-actin based on the results shown in A-B. The area of overlap between Flag and F-actin was compared with the total area expressing Flag to obtain the F-actin-positive Flag/total Flag ratio. Mean±SD (n=6 cells, respectively, **p< 0.01). D, Ferm of FRMPD2 co-precipitated with F-actin in a co-sedimentation assay. GST -Ferm or α-actinin (a positive control) were mixed with F-actin, co-precipitated by ultracentrifugation, and stained with Coomassie blue. P, pellet; S, supernatant.

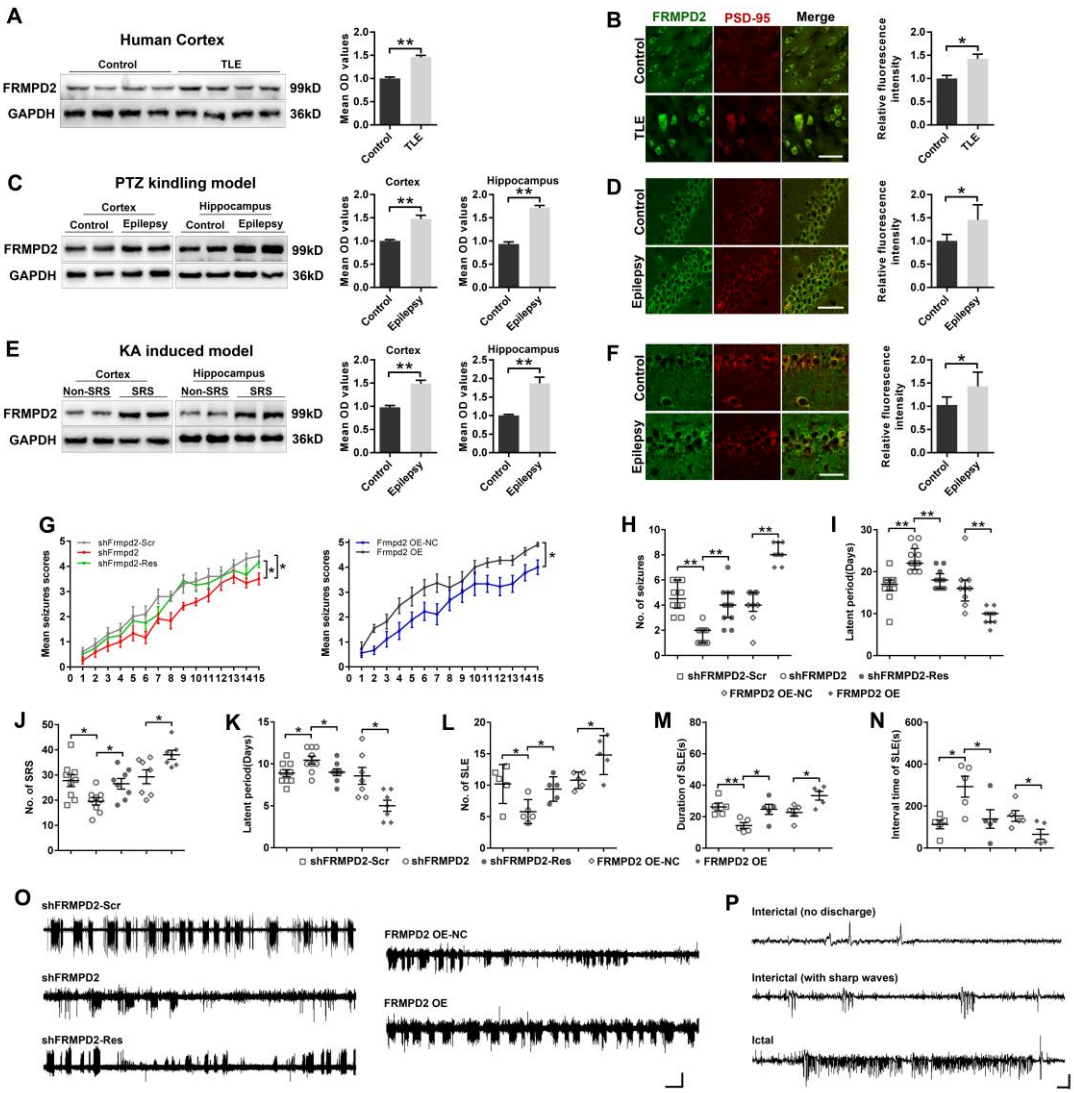

Fig 5. Modulation of FRMPD2 in epilepsy susceptibility.

A, B, FRMPD2 expression of temporal neocortex of TLE patients(n=20) and control patients(n=12) by immunoblot (A) and immunofluorescence staining(B). Bar, 40 μm. C, D, FRMPD2 expression in the hippocampus(C, D) and neocortex(C) in the PTZ induced mice. n=10-11 mice in each group(C). Bar, 40 μm. E, F, FRMPD2 expression in the hippocampus(E, F) and neocortex(E) were compared between the KA-treated mice and control mice without SRS. n=8-11 mice in each group. Bar, 40μm. G-I, Quantitative analysis of daily seizure scores (G), total number of seizures with a score of 4 or 5 (H) during and latency of the first seizure with a score of 4 or 5 (I) in

PTZ induced mice after FRMPD2 knockdown and overexpression. n=9-12 mice in each group. J-K, Quantitative analysis of total number (J) and latency (K) of the first SRSs with a score of 4 or 5 in KA induced mice. n=7-9 mice in each group. L-N, Quantitative analysis of number (L), duration (M) and interval times (N) of seizure like event (SLE) in KA induced mice. n=7-9 mice in each group. O, P, Representative images of SLEs obtained in each group during a 30 min EEG recording. Bar, 100 s, 0.25 mV (O). EEG showed normal baseline, sharp waves in the interictal stage and an SRS in the KA-induced epilepsy model. Bar, 2.5 s, 0.25 mV (P). OD, optical density. Data were shown as the mean±SD or median with interquartile range; *p< 0.05, **p< 0.01.

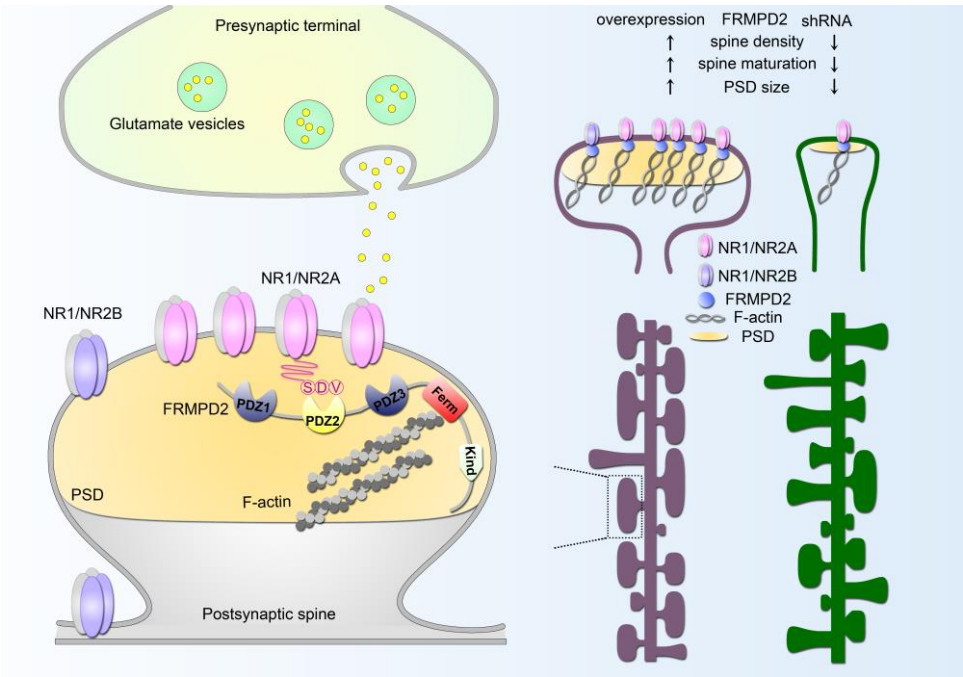

Fig 6. Model demonstrating regulation of FRMPD2 at excitatory synaptic transmission.

Supplementary Methold

Crystallization

GST-PDZ2 (amino acids 934-1027) was expressed in Escherichia coli, BL21(DE3) cells. Cells pellet was sonicated and centrifuged at 5000 rpm. The supernatant was subjected to GST column purification (10 mM Tris, 10 mM GSH, pH 7.4). Pooled fractions were dialyzed with thrombin and passed through a Q-HP column (20 mM Tris, 0-1 M NaCl, 5% glycerol, pH 8.0). Finally, protein fractions were further purified by Superdex 75 columns (20 mM Tris, 5% glycerol, 150 mM NaCl, 2 mM DTT pH 7.4) for crystallization.

Screen kits, including the JCSG-CORE-I-IV (Qiagen) and HR2-144 Index (Hampton), were used to perfrom crystallization screen with the hanging drop method at 18 ºC. The protein (15 mg/ml) was mixed with an equivalent volume (1 µl) of screen buffer. The crystal was grown in 20% PEG3350 and 0.2 M sodium thiocyanate. A single crystal was transferred to the crystallization buffer containing an additional 20% glycerol and flash frozen with liquid nitrogen. The crystal diffracted well at BL19U (Shanghai Synchrotron Radiation Facility, SSRF, China). In all, images for 180° were collected. The data were processed by HKL3000 (Supplemental Table 1). The crystal structure was refined by PHENIX and Coot. The structure was refined to 1.80 Å with R factor 19.76% and R free 24.76%.

Supplementary Figures

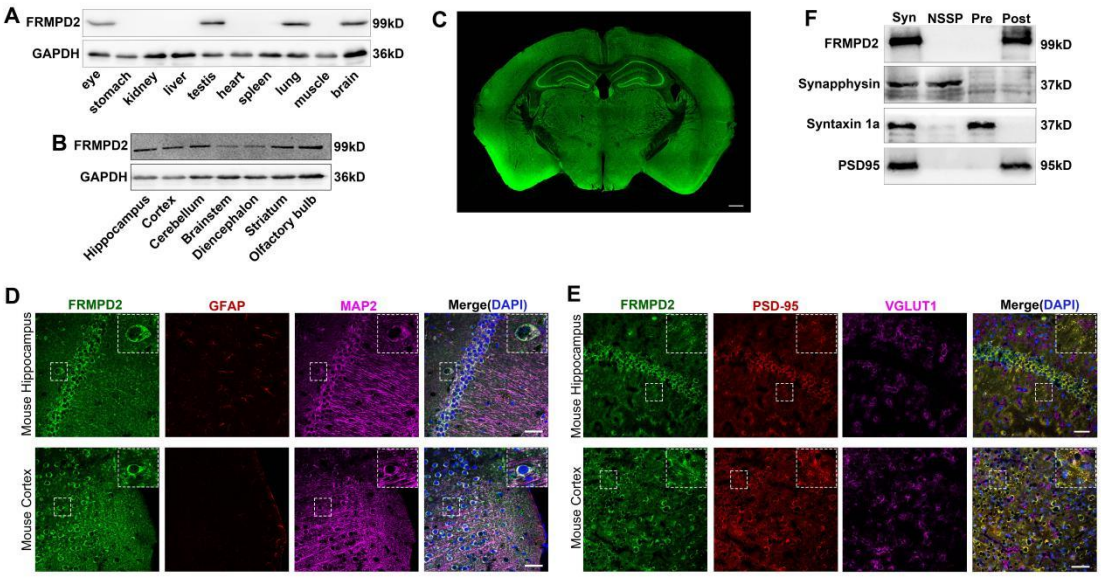

Supplementary Fig 1. Expression patterns of the FRMPD2 protein.

A, FRMPD2 protein is located in the mouse brain, eyes, testes and lungs. B, The brain-specific expression of the FRMPD2 protein was revealed in adult mouse tissue homogenates. C, The FRMPD2 protein has a widespread distribution pattern in adult mouse brain slices. Bar, 500 μm. D, FRMPD2 was present in MAP2-positive neuronal dendrites but not in GFAP-positive glial cells as determined by immunofluorescence staining. Bar, 40 μm. E, FRMPD2 co-localized with the postsynaptic marker PSD95 but not with the presynaptic marker VGLUT1 in the mouse hippocampus and cortex. Bar, 40 μm. F, Immunoblot of the synapse fraction (Syn) showing that FRMPD2 was preferentially distributed in the postsynaptic fraction (Post) rather than in the presynaptic (Pre) or non-synaptic synaptosomal proteins (NSSP) fraction. Anti-synapphysin, anti-syntaxin 1a and anti-PSD95 were used as markers for ultrasynaptic fraction to verify that the purity of the preparation was higher than 90%. The blots were representative of 4-6 analyses.

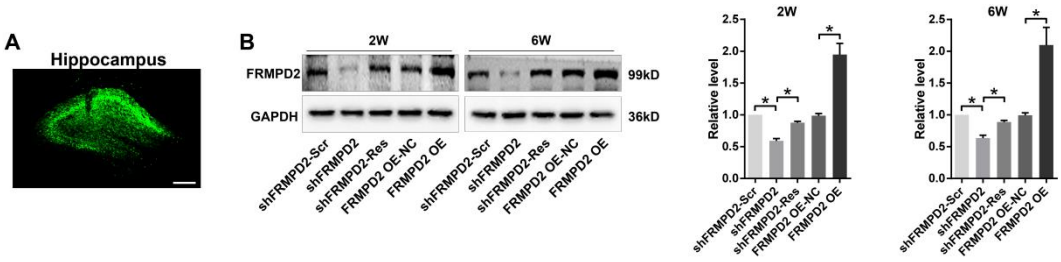

Supplementary Fig 2. Alteration of FRMPD2 protein levels in the hippocampus by LV injection.

A, Lentiviral vector (LV)-encoding green fluorescent protein (GFP) was detected in the mouse hippocampus following the injection of LV. Bar, 250 μm. B, Hippocampal FRMPD2 protein expression levels were detected in FRMPD2 knockdown or overexpression mice on the 2 and 6 weeks after LV injection. Data were shown as mean±SD and analyzed by Student's t test, n=5 mice, *$p < 0.05$.

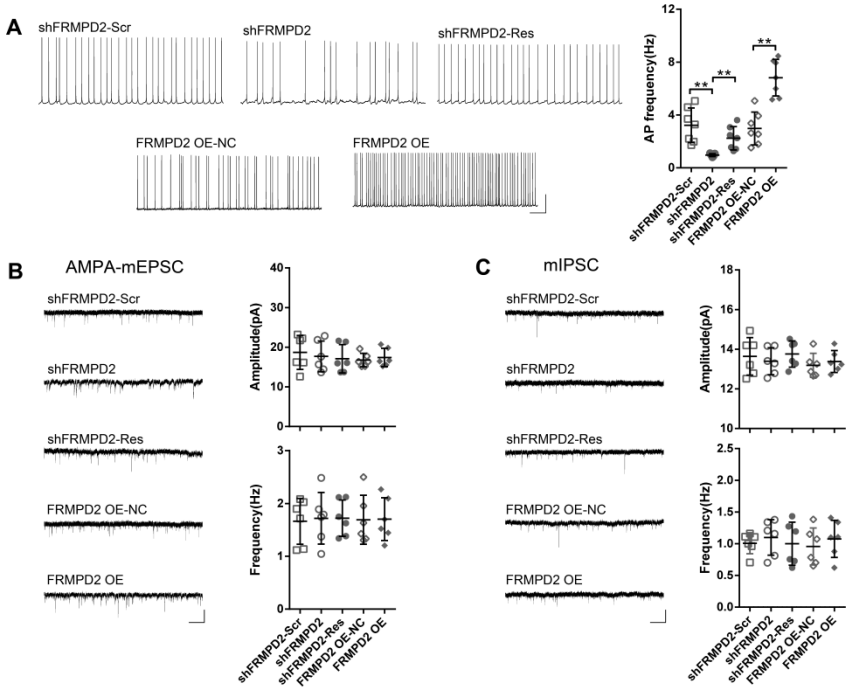

Supplementary Fig 3. Effects of FRMPD2 on electrophysiology of CA1 neurons in mouse hippocampal brain slices.

A, The frequency of spontaneous AP was compared after FRMPD2 knockdown or overexpression. Bar, 1 s, 25 mV. B, C, FRMPD2 had no significant effect on the amplitude or frequency of AMPAR mEPSCs (B) and mIPSCs (C). Bar, 1 s, 20 pA. Data were shown as mean±SD and analyzed by Student's *t* test, n=6-7 neurons of 3 mice, **p< 0.01.

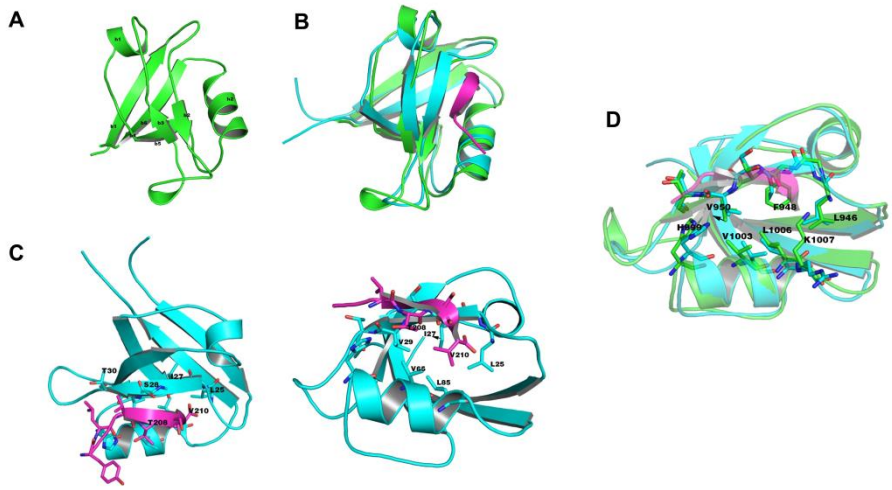

Supplementary Fig 4. Crystal structure of FRMPD2 PDZ2 domain.

A, The crystal structure of a compact globular fold in the ligand-free FRMPD2 PDZ2 domain (PDB ID: 5ZDS) was shown. B, The crystal structure of the FRMPD2 PDZ2 domain (green) was shown aligned to that of the PDZ2-peptide template structure (cyan and magenta) (PDB ID: 1VJ6). C, A template of PDZ2-peptide (cyan and magenta) interaction (PDB ID: 1VJ6). D, The binding pocket alignment between FRMPD2 PDZ2 crystal structure (green) and PDZ2 template (cyan).

Supplementary Table 1. Data collection and refinement statistics of PDZ2 of FRMPD2.

	PDZ2
Data collection	
Wavelength(Å)	0.9786
Resolution range(Å)	50-1.58 (1.64-1.58)[a]
Space group	P 2_1 2_1 2
Unit cell dimensions	
a, b, c(Å)	32.200, 48.179, 56.845
α, β, γ(°)	90, 90, 90
No. of reflections	80345
No. unique reflections	12699 (1248)
Multiplicity	6.3 (6.4)
Completeness (%)	99.7 (100)
Mean I/σ (I)	22.52(7.70)
R-meas	0.065(0.268)
Refinement	
Resolution range(Å)	50-1.8 (1.86-1.8)
No. of reflections	8610 (849)
No. of reflections used for R-free	860 (85)
R-work	0.1980 (0.2202)
R-free	0.2347 (0.2630)

No. of non-hydrogen atoms	810
Macromolecules	658
Protein residues	88
R.m.s.d.	
Bond lengths(Å)	0.005
Bond angles(°)	0.83
Ramachandranplot(%)	
Allowed regions	1.1
Outliers	0
Average B-factor	13.71
Macromolecules	11.25
Solvent	24.37

[a]Statistics for the highest-resolution shell are shown in parentheses. No., number, r.m.s.d., root mean squared deviation.

Supplementary Table 2. Clinical details of TLE patients and control patients

Cases	Sex	Age (years)	Duration (years)	Seizure type	Preoperative AEDs consumption	Resected tissue	Pathological diagnosis
E1	F	27	14	SGS	PHT, VAP, CZP	RTN	G
E2	F	13	4	SGS	CBZ, TPM, VPA	LTN	NL, ND, G
E3	F	15	3	CPS, SE	CBZ, TPM, LTG	RTN	G
E4	M	47	29	SGS	VPA, PHT, TPM, PB,LTG	RTN	G
E5	M	28	3	SGS	PB, CBZ, VPA	LTN	NL, ND, G
E6	F	38	12	SGS	CBZ, TPM, VPA	LTN	NL, ND, G
E7	F	29	27	SGS	CBZ, VPA, LTG	RTN	NL, G
E8	F	37	7	CPS, GTCS	CBZ, TPM, VPA	LTN	NL, G
E9	M	32	19	CPS	CBZ, TPM, PB,VPA	LTN	ND, G
E10	M	30	10	SGS	CBZ, VPA, PHT	LTN	NL, ND, G
E11	F	11	4	SGS	VPA, CBZ, TPM, LTG	RTN	G
E12	M	22	7	SGS, SPS	VPA, TPM, LTG	LTN	NL, G
E13	F	44	12	CPS	VPA, PHT, LTG	RTN	NL, G
E14	M	33	9	CPS	VPA, PHT, LTG	RTN	G
E15	M	17	3	SGS	PHT, PB, CBZ, LTG	LTN	NL, G
E16	F	14	5	SGS, CPS	VPA, CBZ, PHT, PB	RTN	NL, ND
E17	M	24	3	SGS, CPS	VPA, TPM, OXC	RTN	G

E18	F	33	10	SGS	CBZ, PHT	RTN	G
E19	M	29	14	CPS	VPA, TPM, CBZ, LTG,PHT	LTN	NL, ND, G
E20	M	24	11	CPS	VPA, PHT, CBZ	RTN	NL, G
C1	F	14	0	None	None	LTN	N
C2	F	25	0	None	None	RTN	N
C3	F	32	0	None	None	RTN	N
C4	M	28	0	None	None	RTN	N
C5	M	21	0	None	None	LTN	N
C6	M	54	0	None	None	LTN	N
C7	F	38	0	None	None	RTN	N
C8	M	50	0	None	None	RTN	N
C9	M	43	0	None	None	LTN	N
C10	F	33	0	None	None	LTN	N
C11	M	31	0	None	None	RTN	N
C12	F	15	0	None	None	LTN	N

AEDs, antiepileptic drugs; E, epilepsy; C, control; F, female; M, male; CPS, complex partial seizure; SPS, simple partial seizure; SGS, secondarily generalized seizure; GTCS, generalized tonic clonic seizure; SE, status epilepticus; CBZ, carbamazepine; CZP, clonazepam; LTG, lamotrigine; OXC, oxcarbazepine; PB, phenobarbital; PHT, phenytoin; TPM, topiramate; VPA, valproate; LTN, left temporal neocortex; RTN, right temporal neocortex; NL, neuron loss; ND, neuron degeneration; G, gliosis; N, normal.